

## Frontogenesis Processes in the Middle and Upper Troposphere

KEITH M. HINES AND CARLOS R. MECHOSO

*Department of Atmospheric Sciences, University of California—Los Angeles, Los Angeles, California*

(Manuscript received 16 March 1990, in final form 9 November 1990)

### ABSTRACT

Basic issues regarding upper-level frontogenesis addressed in this paper are: (i) simulated frontogenesis influenced by the initial flow, (ii) upper-level frontogenesis as essentially a two-dimensional process, and (iii) frontal-scale positive feedback between vertical advection of momentum and vorticity advection by the ageostrophic wind, which is important for the intensification of upper-level frontal zones. The methodology for investigation is based on analysis of simulated upper-level frontogenesis with a three-dimensional primitive-equation model. The model is a simplified version of the UCLA GCM, with 21 layers in the vertical, horizontal resolution of  $1.2^\circ \text{ lat} \times 1.5^\circ \text{ long}$ ; a  $60^\circ$  sector of one hemisphere as periodic domain; and physics reduced to horizontal diffusion and dry convective adjustment. Simulations initialized with jet streams symmetric about the latitude of maximum wind at each pressure level produce—in the middle troposphere—the strongest frontal zones downstream of the trough of growing baroclinic waves. Strongest upper-level frontal zones originating upstream of the wave trough, as observed, are produced when initial jet streams and perturbations are chosen so that the growing waves have small meridional phase tilt in the initial stages.

In the simulations, tilting associated with divergence of the across-jet ageostrophic flow is the dominant frontogenetical process upstream of the wave trough. Further, tilting associated with divergence of the ageostrophic wind along the jet also contributes to frontogenesis, but to a lesser extent. The former result is similar to that obtained with two-dimensional models in which frontogenetical vertical motions are associated with divergence of the ageostrophic wind across the front.

No definitive evidence is found proving that the simulated frontogenesis is enhanced by a positive-feedback process involving vertical advection of momentum and vorticity advection by the ageostrophic wind. It is found, however, that both of these processes are nonnegligible contributors to the frontal intensification.

### 1. Introduction

This is a study of the frontogenesis processes in the middle troposphere and upper troposphere (i.e., upper-level or internal frontogenesis). Newton and Trevisan (1984a) define frontogenesis as the formation of a sloping frontal layer comprising increased baroclinity, vertical and lateral shear, and static stability. (They term clinogenesis to a process that includes all but the latter of these features.) The problem is of long-standing interest in atmospheric dynamics: Palmén (1951) noted the link between frontogenesis and the formation of upper jet streams.

We focus on three basic, albeit largely unresolved, issues regarding upper-level frontogenesis.

(i) Is simulated frontogenesis influenced by the initial flow?

(ii) Many observed features of upper-level frontogenesis are reproduced in two-dimensional simulations.

Is upper-level frontogenesis essentially a two-dimensional process?

(iii) Mudrick (1974) suggests that a positive-feedback process develops during upper-level frontogenesis. The process can be summarized by the following steps (see Fig. 1). Consider cross-isobar flow on the confluence side of a jet. This flow allows for negative vorticity advection, which increases with height and enhances the subsidence below the jet. The tilting effect due to this subsidence intensifies the across-jet vorticity gradient, tightening the jet. To our knowledge, the existence of this positive-feedback process has not been conclusively proven or disproven. Further, no other process of a similar kind has been proposed. The following question, therefore, remains open: is a frontal-scale positive feedback between vertical advection of momentum and vorticity advection by the ageostrophic wind at work in the intensification of upper-level frontal zones?

Our strategy is based on detailed analysis of simulated evolutions of unstable baroclinic waves with a three-dimensional primitive-equation (PE) adiabatic model. In this scenario, frontogenesis is an integral component of the evolutions. Our choice of the adi-

---

*Corresponding author address:* Dr. Keith M. Hines, Department of Atmospheric Sciences, University of California—Los Angeles, Los Angeles, CA 90024.

## Positive-Feedback Mechanism for Upper-Level Frontogenesis (Mudrick, 1974)

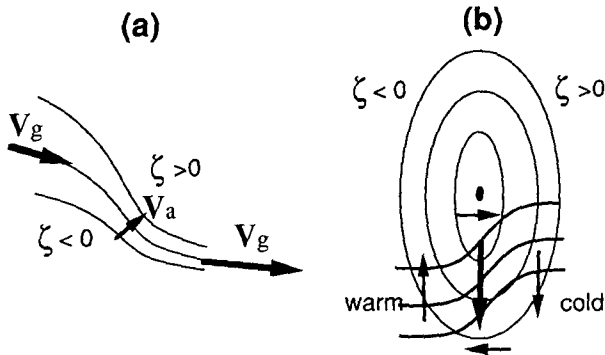


FIG. 1. Positive-feedback mechanism for upper-level frontogenesis from Mudrick (1974). (a) Horizontal flow pattern in the upper troposphere along a jet stream. Solid lines are contours of the geopotential field. Thick arrows represent the geostrophic wind increasing downstream. The thin arrow represents the across-jet ageostrophic wind. (b) Cross section perpendicular to the jet stream. Thin lines are isobars. Thick lines are isentropes. Thin arrows depict a direct solenoidal circulation. The thick arrow represents subsidence enhanced by the positive feedback involving negative vorticity advection and tilting.

abatic framework, as well as that of the methodology for analysis, is based on previous observational, theoretical, and modeling work on the subject.

We begin section 2 with a review of our current understanding of upper-level frontogenesis in order to provide the motivations for our study. Section 3 describes the numerical model used. Section 4 deals with the impact of the model's resolution on simulated frontogenesis. The procedure followed to determine appropriate initial conditions for the simulation of frontal zones resembling those observed, and the analysis of the simulated frontogenetical processes are presented in section 5. A summary of the results of this study and the conclusions are given in section 6.

## 2. Observational and modeling studies of upper-level fronts

### a. Observational studies

The reader is referred to Keyser and Shapiro (1986) for a comprehensive review of observational, theoretical, and modeling work on upper-level fronts. The following review is restricted to the aspects most relevant to our specific objectives.

The mechanisms involved in tropospheric frontogenesis are simply illustrated by the equation for the rate of change of the horizontal potential temperature gradient squared for an ideal fluid,

$$\frac{d}{dt}(\nabla\theta)^2 = -(\nabla \cdot \mathbf{v})(\nabla\theta)^2 \quad \text{I-}\theta$$

$$+ (\cos 2\delta)D(\nabla\theta)^2 - 2\frac{\partial\theta}{\partial p}\nabla\omega \cdot \nabla\theta, \quad \text{II-}\theta \quad \text{III-}\theta \quad (1)$$

where  $t$  is the time,  $\nabla$  is horizontal gradient operator,  $p$  is pressure,  $\theta$  is potential temperature,  $\mathbf{v}$  is horizontal velocity, and  $\omega$  is vertical velocity. The variable  $\delta$  is the angle between  $\nabla\theta$  and the axis of contraction for the fluid motion (or the angle between lines of constant potential temperature and the axis of dilatation). The deformation parameter  $D$  for the horizontal component of the motion is defined (in Cartesian coordinates) as,

$$D = \left[ \left( \frac{\partial u}{\partial x} - \frac{\partial v}{\partial y} \right)^2 + \left( \frac{\partial u}{\partial y} + \frac{\partial v}{\partial x} \right)^2 \right]^{1/2}, \quad (2)$$

where  $u$  and  $v$  are the zonal and meridional wind components, respectively.

According to (1), changes in  $(\nabla\theta)^2$  are due to horizontal divergence and deformation (represented by I- $\theta$  and II- $\theta$ , respectively) and tilting (represented by III- $\theta$ ). The corresponding signs imply that horizontal convergence and divergence are frontogenetical and frontolytical, respectively. Horizontal deformation may be frontogenetical or frontolytical depending on the orientation of the thermal field to the deformation field; namely  $\delta$  smaller or larger than  $\pi/4$ . Tilting is frontogenetical if the vertical circulation is thermally indirect ( $\nabla\omega \cdot \nabla\theta > 0$ ).

Namias and Clapp (1949) discuss the formation of jet streams in confluent flow. Horizontal deformation (II- $\theta$ ) is the dominant frontogenetical process in this case. The associated solenoidal circulation (III- $\theta$ ) is frontolytical. The height-dependent divergence (I- $\theta$ ) of the across-jet circulation favors formation of a front sloping with height over the colder air.

Several authors discuss the formation of fronts in association with synoptic-scale waves (Reed and Sanders 1953; Newton 1954; Reed 1955; Staley 1960; Bosart 1970; Shapiro 1970; Uccellini et al. 1985). Tilting (III- $\theta$ ) is an important frontogenetical process in this case. Consider a diffluent upper-level trough of a synoptic-scale wave with strong flow upstream and weaker flow downstream. The corresponding vertical velocity field (Krisnamurti 1968) includes sinking and rising upstream and downstream of the trough, respectively. In these conditions, (1) shows that tilting contributes to frontogenesis on the cold-air side of the flow upstream of the trough.

Bosart (1970) finds that the dominant frontogenetical process can vary in time during the evolution of the front. Around the location where frontogenesis

starts, upstream of the trough, the dominant frontogenetical effect is tilting, with a weaker contribution by deformation. Later on, tilting is frontogenetical upstream of the front and frontolytical farther downstream, while deformation remains frontogenetical throughout the entire frontal zone.

The vertical velocity field observed in association with upper-level fronts at about 500 mb shows a subsidence maximum on the warm edge of the frontal zone, roughly below the jet core (Reed and Sanders 1953; Reed 1955; Bosart 1970; Uccellini et al. 1985). This implies a thermally indirect local circulation. Reed (1955) also finds that the circulation is direct solenoidal in the warm air outside the frontal zone. Shapiro (1970) observes indirect circulation on a long path parallel to the flow upstream of the trough where the front forms. The subsidence maximum is on the order of  $0.1 \text{ m s}^{-1}$ , which is consistent with estimates obtained in a scale analysis.

Observational studies examine the processes that modify the vorticity and other quantities in upper-level fronts. The equation for the rate of change of  $\zeta$ , the vertical component of relative vorticity, is

$$\frac{d}{dt} \zeta = -(\zeta + f) \nabla \cdot \mathbf{v} + k \cdot \left( \frac{\partial \mathbf{v}}{\partial p} \times \nabla \omega \right) - \nabla f \cdot \mathbf{v}, \quad (3)$$

I- $\zeta$                       II- $\zeta$                       III- $\zeta$

where  $f$  is the Coriolis parameter and  $\mathbf{k}$  is the vertical unit vector. According to (3), changes in vorticity are associated with horizontal divergence (represented by I- $\zeta$ ), tilting (represented by II- $\zeta$ ), and the variation of the Coriolis parameter with latitude ( $\beta$  effect, represented by III- $\zeta$ ).

Reed and Sanders (1953) find that the relative vorticity in the frontal region between 400 and 500 mb increases due to tilting, which is an order of magnitude larger than the planetary vorticity advection and divergence terms. The divergence term is dominant at higher and lower levels. Staley (1960) finds that vorticity at 500 mb increases on the cold side and decreases on the warm side of the frontal zone, primarily by vertical advection and tilting. At this level, contributions of vertical advection, tilting, and divergence are of the same order of magnitude. Newton (1954) studies changes in vorticity, vertical shear, horizontal temperature gradient, and static stability for parcels passing through a frontal zone. He finds that the dominant processes responsible for these changes vary with height. Tilting changes the horizontal temperature gradient and the vorticity in the midtroposphere, while divergence and deformation do it near both the tropopause and the surface. In the middle and lower troposphere, changes in vertical shear and static stability are controlled primarily by vertical variations of the across-jet ageostrophic wind. Palmén and Newton (1969) note that vertical shear and stability are generated or dissi-

pated mainly by vertical variations of the across-jet circulation, essentially involving nongeostrophic motions. Uccellini et al. (1985) find that convergence increases vorticity and decreases static stability of subsiding stratospheric air.

Shapiro (1970) estimates, based on a scale analysis, that within the frontal zone divergence and tilting terms are the largest among those on the right-hand side of (3), and that they tend to compensate for each other. Keyser and Shapiro (1986) point out that cyclonic shear is strong in the front and near the intersection of the front and the tropopause. Weaker anticyclonic shear is on the warm side of the jet.

A distinct characteristic of upper-level fronts is their association with the tropopause folding process. Observational data on humidity, ozone, and Ertel's potential vorticity show that air with characteristics of the lower stratosphere can be found deep into the troposphere within upper-level frontal zones (Reed and Sanders 1953; Reed 1955; Reed and Danielsen 1959; Staley 1960; Danielsen 1968; Bosart 1970; Shapiro 1978; Uccellini et al. 1985). Reed (1955) and Uccellini et al. (1985) observe wedges of air with high potential vorticity resembling that in the stratosphere as low as 700–800 mb. Staley (1960) indicates that stratospheric air can descend to within 5000 ft of the surface within 24 h.

### b. Two-dimensional models of frontogenesis

Typically, the length scale along the front is much longer than that across the front. This suggests a two-dimensional approach, in which curvature effects along the front are neglected. Two-dimensional models of frontogenesis focus on the circulations in vertical cross sections (transverse, across-front circulations). They generally use the Sawyer–Eliassen equation as a diagnostic tool (Eliassen 1962). The Sawyer–Eliassen equation is

$$L(\chi) = \frac{\partial v_g}{\partial y} \cdot \nabla \theta = \frac{\partial v_g}{\partial y} \frac{\partial \theta}{\partial y} + \frac{\partial u_g}{\partial y} \frac{\partial \theta}{\partial x}, \quad (4)$$

where  $\chi$  is the streamfunction of the across-front circulation;  $L(\chi)$  is a second-order linear differential operator;  $x$  and  $y$  are the along-front and the across-front coordinates, respectively; and the subscript  $g$  identifies geostrophic quantities. The first and second terms on the right-hand side of (4) are the geostrophic confluence and geostrophic shear forcings, respectively.

In the two-dimensional framework, the temperature and wind fields are written in the following manner,

$$\theta(x, y, p, t) = \bar{\theta} + \bar{\theta}_1(x, p, t) + \theta'(y, p, t), \quad (5)$$

$$\mathbf{v}(x, y, p, t) = \bar{\mathbf{v}}(x, y) + \bar{\mathbf{v}}_1(p, t) + \mathbf{v}'(y, p, t). \quad (6)$$

Overbars and primes indicate prescribed (basic state) and dependent (perturbation) quantities, respectively. Term  $\bar{\theta}$  is a constant,  $\bar{\theta}_1$  represents the along-front potential temperature variation, and  $\theta'(y, p, t)$  represents the across-front potential temperature structure. Also  $\bar{v}(x, y)$  corresponds to a deformation field, and  $\bar{v}_1(p, t)$  is obtained by solving the appropriate equations with  $\bar{\theta}$ ,  $\bar{\theta}_1$ , and  $\bar{v}$ . Term  $v'(y, p, t)$  corresponds to the jet stream and the across-front vertical circulation. An exponential decay of the alongfront potential temperature gradient is required for dynamical consistency if  $\bar{v}$  has constant (space and time) deformation.

Hoskins (1971, 1972), Hoskins and Bretherton (1972), and Buzzi et al. (1981) use two-dimensional models based on the geostrophic momentum approximation (Hoskins 1975) to examine frontogenesis in the case  $\bar{\theta}_1 = \bar{v}_1 = 0$ . In this case, across-front circulations are forced through the confluence  $\partial v/\partial y$  and the across-front temperature gradient  $\partial\theta/\partial y$ . Hoskins (1971, 1972) and Hoskins and Bretherton (1972) use models consisting of two fluids of different potential vorticity, in which the interface represents the tropopause. Buzzi et al. (1981) use a model with continuous potential vorticity distribution. All obtain weak frontogenesis developing near the tropopause due to horizontal deformation. The corresponding cross-front circulations are thermally direct and, accordingly, horizontal temperature gradients are weak in the middle troposphere.

Keyser and Shapiro (1986) recognize four stages in the origin and evolution of an upper-tropospheric jet/frontal system on a short-wave trough moving through a synoptic-scale wave evolving in time. Stage 1 is analogous to the process described by Namias and Clapp (1949), as there is confluence between the synoptic-scale ridge and the trough. In stage 2, the front is upstream of the trough, near the inflection point of the longer wave, which is growing and producing cold advection in the frontal zone. Tilting may be frontogenetical at this stage. In stage 3, the front is at the base of the longer wave trough, which is no longer growing. In stage 4, the front is in confluent flow downstream of the trough of the longer wave, which is decaying. Tilting may be frontolytic at this stage.

Keyser and Pecnick (1985) use a two-dimensional, primitive-equation model to analyze the structure of the flow in the first, second, and fourth stages. Stage 1 corresponds to the pure confluence case ( $\bar{v}_1 = \bar{\theta}_1 = 0$ ). Results in this case resemble those of Hoskins and Bretherton (1972) and Buzzi et al. (1981), as direct circulation, weak upper-level frontogenesis, and weak tropopause folding develop. Stage 4 corresponds to confluence with warm advection along the front ( $\partial\bar{\theta}_1/\partial x < 0$ ). Stronger frontogenesis and direct circulation are obtained in this case as both stretching and shearing deformation contribute to the frontogenesis.

Interestingly, the case corresponding to stage 2 (i.e., cold advection along the front) is the closest to capturing outstanding observed features. A well-defined front extends from the tropopause into the middle troposphere. Frontogenesis develops due to tilting, whereas horizontal deformation is frontolytic. The maximum subsidence is on the warm edge of the frontal zone as the direct circulation cell shifts toward the warm air. Vertical velocity is stronger than in both the pure confluence and warm advection cases. The tropopause folds to about 700 mb. These results confirm Shapiro's (1981) hypothesis that forcing involving the horizontal shear  $\partial u/\partial y$  and the alongfront temperature gradient  $\partial\bar{\theta}/\partial x$  may shift the vertical circulation laterally so that it becomes locally indirect in the frontal zone.

Reeder and Keyser (1988) compare results of two-dimensional models based on the anelastic, geostrophic-momentum, and quasi-geostrophic system of equations (AN, GM, and QG models, respectively) all with across-front circulation forced by confluence and shear. They find substantial differences between the results of the QG and the other models. These differences are attributed to the neglect of vertical advection of momentum in the quasi-geostrophic system of equations. Reeder and Keyser (1988) also find that the differences between the results of the AN and GM models are generally small when the along-front temperature gradient is small. The differences increase with increasing along-front temperature gradients, however, since the across-front circulation tends to increase in magnitude and shift its location. The nondivergent, along-front ageostrophic wind modifies the dynamics of the AN model through its horizontal shear.

In summary, two-dimensional models examine frontogenesis with prescribed height and time independent forcing due to confluence from  $\bar{v}$ . They produce frontogenesis resembling that observed, especially if they include shear forcing associated with cold advection along the front. Models based on the geostrophic-momentum approximation are significantly more successful than those with the quasi-geostrophic approximation in capturing major features of two-dimensional simulations of frontogenesis, performed with models based on the PE and anelastic approximations.

### *c. Three-dimensional models of frontogenesis*

In the three-dimensional approach, frontogenesis is obtained during simulated evolutions of baroclinic waves. The three-dimensional formulation allows for curved trajectories dynamically associated with ageostrophic flow parallel to the geostrophic wind.

Mudrick (1974) investigates upper-level frontogenesis using a three-dimensional, adiabatic, PE, Boussinesq model. The model domain is a midlatitude,  $\beta$ -plane channel with periodic boundary conditions in

the zonal direction. The initial conditions consist of the superposition of a zonally symmetric jet stream, nearly symmetric about the latitude of maximum wind, and its most unstable, quasi-geostrophic perturbation.

In the simulation, an upper-level front forms upstream of the wave trough and extends to around its base. The strongest temperature gradient and wind speed develop slightly upstream of the base of the trough. There is a maximum of subsidence below the jet core on the warm side of the frontal zone. The subsidence is associated with the increase in height of the negative vorticity advection. A diagnostic analysis reveals that horizontal deformation is frontogenetical in the frontal zone.

The results are compared with those of a QG version of the model from the same initial conditions. There are several similarities and important differences between the PE and QG simulations. The locations of maxima and minima of vertical velocity are in broad qualitative agreement. Vertical motions, however, tend to have larger magnitude in the PE than in the QG simulation. Moreover, the QG simulation does not produce significant upper-level frontogenesis. This suggests that the vertical motion field in the PE simulation is largely controlled by processes included in the QG model, but that the contribution of nongeostrophic effects can be locally important. It also suggests that dynamical processes excluded from the QG model are important for the intensification of upper-level frontal zones.

In the Introduction, we sketched the positive-feedback mechanism for upper-level frontogenesis proposed by Mudrick (1974, see Fig. 1). It is now described in more detail. Upstream of the trough and below the jet core, the across-jet advection of negative vorticity by the ageostrophic wind increases with height just as the magnitude of both the across-jet vorticity gradient and the ageostrophic flow towards lower pressure do. Analysis of a PE form of the  $\omega$  equation shows that across-jet advection of negative vorticity increasing with height contributes to subsidence below the jet core. With these conditions, tilting enhances the across-jet vorticity gradient by increasing the cyclonic and anticyclonic shears on the flanks below the jet core [see (3)]. The process feeds back upon itself as increased across-jet vorticity gradient results in increased across-jet vorticity advection and further subsidence below the jet. In principle, this mechanism could exist in two-dimensional models forced only by confluence, although no examples are reported in the literature.

A conceptual, three-dimensional model of upper-level frontogenesis associated with a baroclinic wave is presented by Newton and Trevisan (1984a) and further discussed by Keyser and Shapiro (1986). There are two basic assumptions in this approach: 1) tightening of the horizontal temperature gradient is essentially the passive result of large-scale processes, and 2) pro-

cesses involving the along-jet component of the ageostrophic wind can be treated independently of those involving the across-jet component.

Newton and Trevisan (1984a) treat the effect of along-jet ageostrophic motions within the framework of a gradient wave. For a gradient wave, the wind is supergeostrophic in the ridge and subgeostrophic in the trough. Consequently, upper-tropospheric convergence and midtropospheric subsidence are expected on the jet upstream of the trough. According to (1), therefore, the tilting effect associated with the indirect circulation on the cold side of the subsidence maximum below the jet core contributes to tightening of the horizontal temperature gradient. Divergence of along-jet ageostrophic wind, is, therefore, important for clinogenesis.

Newton and Trevisan (1984a) examine the effects of flow transverse to a jet streak in its entrance region. Their views are consistent with those provided by two-dimensional models in the case  $\bar{v}_1 = \bar{\theta}_1 = 0$  [see (5) and (6)]. In the midtroposphere, therefore, the across-jet ageostrophic flow is part of a direct circulation in which frontolytic effects of tilting are approximately compensated by the frontogenetic effect of confluence. On the other hand, this direct circulation produces an increase in static stability (a defining element of upper-level frontogenesis) in the entrance region. Thus, frontogenesis is favored when an entrance region of a jet streak is located in the region of clinogenesis upstream of the wave trough.

In a companion paper, Newton and Trevisan (1984b) examine upper-level frontogenesis simulated using a three-dimensional,  $\beta$ -plane, adiabatic, PE model with the isentropic coordinate and periodic boundary conditions. The initial conditions consist of a zonal jet stream sloping poleward with height. The initial cyclonic shear is larger than the anticyclonic shear. A small perturbation is initially superimposed to the zonal jet.

As the unstable wave grows, upper-level frontogenesis develops upstream of the trough on the indirect circulation side of maximum subsidence. In the midtroposphere, wind speed increases downstream in the region of subsidence to a maximum in the trough. Wind canting (i.e., turning of the wind direction with height) in the frontal zone is consistent with cold advection, as discussed in the companion paper and Keyser and Pecnick (1985). This simulation conforms qualitatively to the  $f$ -plane simulation of Keyser et al. (1989).

Newton and Trevisan (1984b) quantitatively examine changes in simulated properties for the frontal entrance region at 500 mb. They find that confluence and tilting increase the horizontal temperature gradient. Geostrophic and ageostrophic canting increase the vertical shear. Divergence and ageostrophic canting also increase the static stability, while tilting enhances

the vorticity pattern. These findings are supportive of their conceptual model of frontogenesis. They did not, however, analyze separately the contributions to tilting by the vertical velocity associated with the along-jet and across-jet variations of the horizontal velocity.

The use of potential temperature as the vertical coordinate is very convenient for three-dimensional simulations of frontogenesis (Shapiro 1975). Such simulations have been performed by Shapiro (1975) and Buzzi et al. (1977) with  $\beta$ -plane models. The latter authors speculate, from the across-jet circulation obtained in their results, that the mechanism described in Mudrick (1974) may be present in their simulation.

In summary, simulations of upper-level frontogenesis have been performed with three-dimensional models. The results have suggested that frontogenesis may be enhanced by a positive-feedback process involving vertical advection of momentum and vorticity advection by the ageostrophic wind. The results have also been used in support of a conceptual model of frontogenesis. In both cases, not all terms in the model equations that are considered as crucial for the corresponding processes to develop were evaluated quantitatively and compared with others.

### 3. Description of the model

The model used in this study is a simplified version of the UCLA General Circulation Model (GCM) described in Suarez et al. (1983) and Mechoso et al. (1985). In this version, the physical parameterizations are reduced to dry convective adjustment and horizontal diffusion. The prognostic variables of the model are horizontal velocity, potential temperature, and surface pressure. In the horizontal, the equations are discretized using a staggered longitude-latitude C grid (Arakawa and Lamb 1977). The treatment of the horizontal advection terms in the momentum equation is based on the potential enstrophy conserving scheme (Arakawa and Lamb 1981) modified to give fourth-order accuracy for the advection of potential vorticity. The horizontal advection scheme used for the potential temperature is also fourth-order and conserves the global mass integral of its square. Time differencing is by the leapfrog scheme with a Matsuno step included periodically to control the computational mode. Near the poles, selected terms are averaged in longitude in the prognostic equations to maintain computational stability without excessively small time intervals.

The horizontal diffusion is by a nonlinear "eddy viscosity" similar to that used by Manabe et al. (1970), but with a smaller coefficient. We follow this procedure so that the contribution of frontal-scale processes, which motivate this study, to the formation of sharp gradients in the flow is not overdamped. Simulations are analyzed in the period when the "noise" level is still low.

In the vertical, the model uses a modified  $\sigma$ -coordinate system in which the lower boundary and isobaric surfaces above 100 mb are coordinate surfaces. The top of the model atmosphere, at 1 mb, is assumed to be a material surface. Vertical finite differencing (Arakawa and Suarez 1983) guarantees conservation of the global mass integrals of potential temperature and total potential plus kinetic energy under frictionless and adiabatic processes.

Since the primary emphasis of this investigation is on midlatitude processes, the model domain is restricted to one hemisphere. Accordingly, all prognostic variables are assumed symmetric about the equator, except for the meridional wind component, which is assumed antisymmetric about the equator. Further, the model domain is taken as a  $60^\circ$  sector of longitude with periodic boundary conditions. This width of the domain roughly corresponds to the zonal scale of most unstable baroclinic waves for climatological-type zonal jet profiles (Simmons and Hoskins 1977). No orographic elevations are included in the boundary conditions.

Three different horizontal resolutions and two vertical resolutions are used in our simulations. In the horizontal, the "low resolution" is  $4^\circ$  lat  $\times$   $5^\circ$  long, corresponding to the standard low-resolution version of the UCLA GCM; "medium resolution" is  $2.4^\circ$  lat  $\times$   $3^\circ$  long, corresponding to the standard high-resolution version of the UCLA GCM; and "high resolution" is  $1.2^\circ$  lat  $\times$   $1.5^\circ$  long. In the vertical, the "low resolution" is 14 layer and the "high resolution" is 21 layer. The former and latter versions have 7 and 14 levels between the surface and 100 mb, respectively.

Initial conditions for the simulations consist of a zonally symmetric, unstable jet stream. The temperature distribution is obtained from the wind field by using the gradient wind and hydrostatic balance relations, with a reference temperature profile at a specified latitude ( $34^\circ$ ). The jet flows do not satisfy the necessary conditions for either inertial or convective instability.

All simulations start with a "linear" stage. During this stage, which begins after the flow is slightly perturbed, the zonally symmetric component of all prognostic fields is held constant in time. Further, wave components with a zonal wavenumber other than six are filtered out. This procedure allows for the organization of the perturbation into the most unstable structure of the linear system. In the cases presented in this paper, the linear stage is three or four days long. For all results included in this paper, the origin of times corresponds to the beginning of the nonlinear stage.

### 4. Effect of model resolution on simulated frontogenesis

The impact of model horizontal resolution on simulated frontogenesis is evaluated by comparing simu-

lations performed using three horizontal resolutions, the same vertical resolution (14 layer), and identical initial conditions. The initial wind field consists of a broad zonal jet stream centered at 45° latitude given by,

$$\bar{u}(\phi, p) = \hat{u}(p) \sin(\pi \sin^2 \phi), \quad (7)$$

where  $\phi$  is the latitude (Fig. 2). The reference vertical wind profile,  $\hat{u}(p)$ , and the reference vertical temperature profile are taken from Oort (1983) and correspond to winter conditions in the Northern Hemisphere. Maximum wind speed is 39.8 m s<sup>-1</sup> at 45° lat, 200 mb. Notice that  $\bar{u}(\phi, p)$  is symmetric about 45° latitude at each pressure level. The wind is zero at the surface, and sea level pressure is a constant 1000 mb. The flow is perturbed in the latitude band 20°–70° by a high–low couplet in the surface pressure field with maximum amplitude of 1 mb at 45° latitude.

The temperature field at 500 mb for days 2, 3, and 4 of the simulation is shown in Fig. 3. There are no

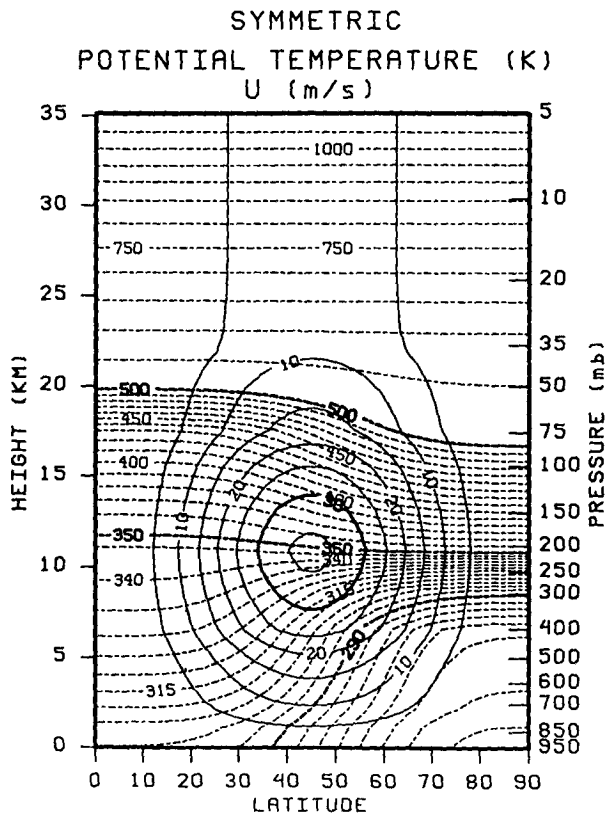


FIG. 2. Latitude–height contour plot of the zonal wind velocity ( $\text{m s}^{-1}$ ) given by Eq. (7) (solid lines) and corresponding potential temperature (K) distribution (dashed lines). Contour interval for wind velocity is 5  $\text{m s}^{-1}$ ; the thick solid line is 30  $\text{m s}^{-1}$ . Contour interval is 5 K below 350 K, 10 K between 350 K and 500 K, and 50 K above 500 K. Thick dashed lines are 290 K, 350 K, and 500 K.

clearly defined frontal structures with the low resolution, and the sharpest potential temperature gradients develop with the high resolution. The evolution of the flow with the different horizontal resolutions is illustrated by the series of contour plots of Ertel's potential vorticity on the surface  $\theta = 300$  K, which goes from the tropopause at the pole to the lower troposphere at the equator (Fig. 4). For all three resolutions there is a tongue of high potential vorticity air flowing equatorward and another tongue of low potential vorticity air flowing polewards. The behavior of the air with high potential vorticity differs markedly with resolution: the lower the resolution, the earlier the southern flow cuts off from the high-latitude sources. The simulated intrusion of stratospheric air into the troposphere appears realistic only with the high resolution.

The vertical resolution in the troposphere of the 14-layer version is rather coarse compared to that used for frontogenesis studies by other authors [Mudrick (1974), and Newton and Trevisan (1984b), both used 20 levels]. Since we wish to contrast the results obtained by these authors with our results, we select the high vertical resolution for our study. Consequently, simulations reported below have been performed with the 1.2° lat  $\times$  1.5° long, 21-layer version of the model.

## 5. Results of the frontogenesis simulations

Figure 3 shows that the simulation with high horizontal resolution produces at 500 mb a region of enhanced potential temperature gradient extending from near the base of the trough downstream into the southwesterly flow. Upstream of the trough, the temperature gradients are weaker. Accompanying the front are strong winds on a geopotential height wave with substantial southwest–northeast phase tilt (Fig. 5). This phase tilt is associated with poleward transport of momentum by the wave. It is known that the meridional phase tilt of unstable baroclinic waves on the sphere may be different than that on the  $\beta$  plane for the same zonal flow (Hollingsworth 1975; Hollingsworth et al. 1976; Simmons and Hoskins 1978). Inspection of the temperature field at lower levels reveals that the enhanced gradient at 500 mb is connected vertically with the surface cold front. Above 500 mb, the strong temperature gradient around the base of the trough weakens with height.

Analysis of the terms in (1) around the base of the trough reveals that the combined effects of horizontal divergence and deformation are frontogenetical at 500 mb and in the lower troposphere. The contribution of tilting is generally frontolytic at 500 mb, except in a small area near the frontal entrance region. There is some apparent similarity between Fig. 3 and the temperature field in Fig. 19d of Keyser and Shapiro (1986), which corresponds to stage 4 in their idealized life cycle of an upper-tropospheric jet/frontal system (see section

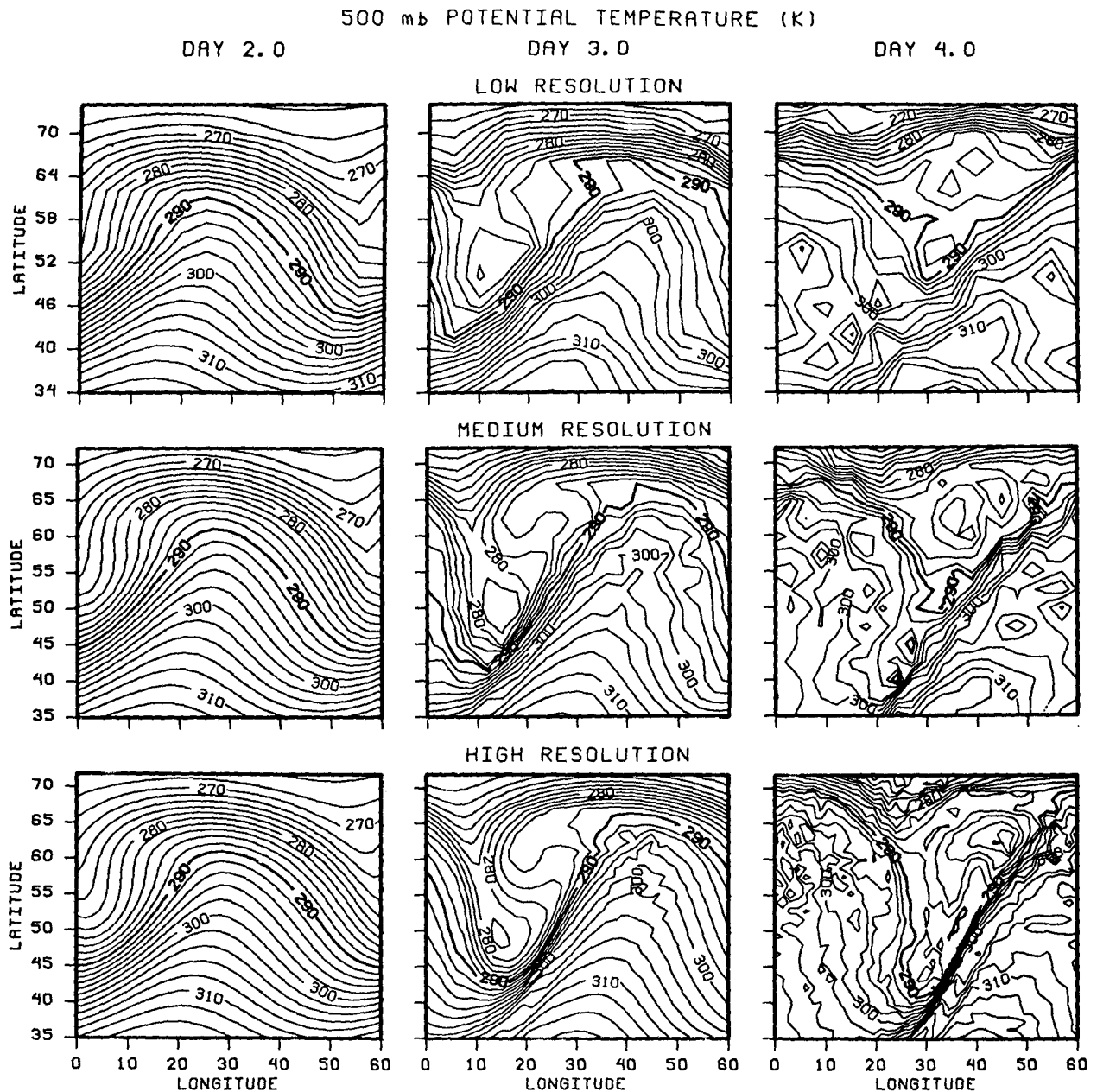


FIG. 3. Longitude-latitude contour plots of potential temperature (K) at 500 mb for days 2, 3, and 4 obtained with the low, medium, and high horizontal resolution versions of the model. Contour interval is 2 K. The thick contour is 290 K.

2a). However, there is warm advection along the jet in that stage, and cold advection in our case. (No similarities are found between our results and stages 1 through 3 either.) This simulated frontogenesis, therefore, has substantial differences with the observed phenomenon and will not be analyzed further in this paper.

A series of simulations were performed from an ensemble of zonal flows with the same vertical profile as (7), but with different meridional profiles, all of them symmetric about the latitude of maximum wind. These

simulations produced similar results in regard to the southwest-northeast phase tilt of the growing waves and frontal structures. This similarity is somewhat expected, since the horizontal structure of the growing unstable waves on the sphere for families of profiles of the type (7) and other symmetric types includes southwest-northeast phase tilt (Hollingsworth 1975; Hollingsworth et al. 1976).

To produce upper-level frontal zones with closer resemblance to those observed, special attention is given

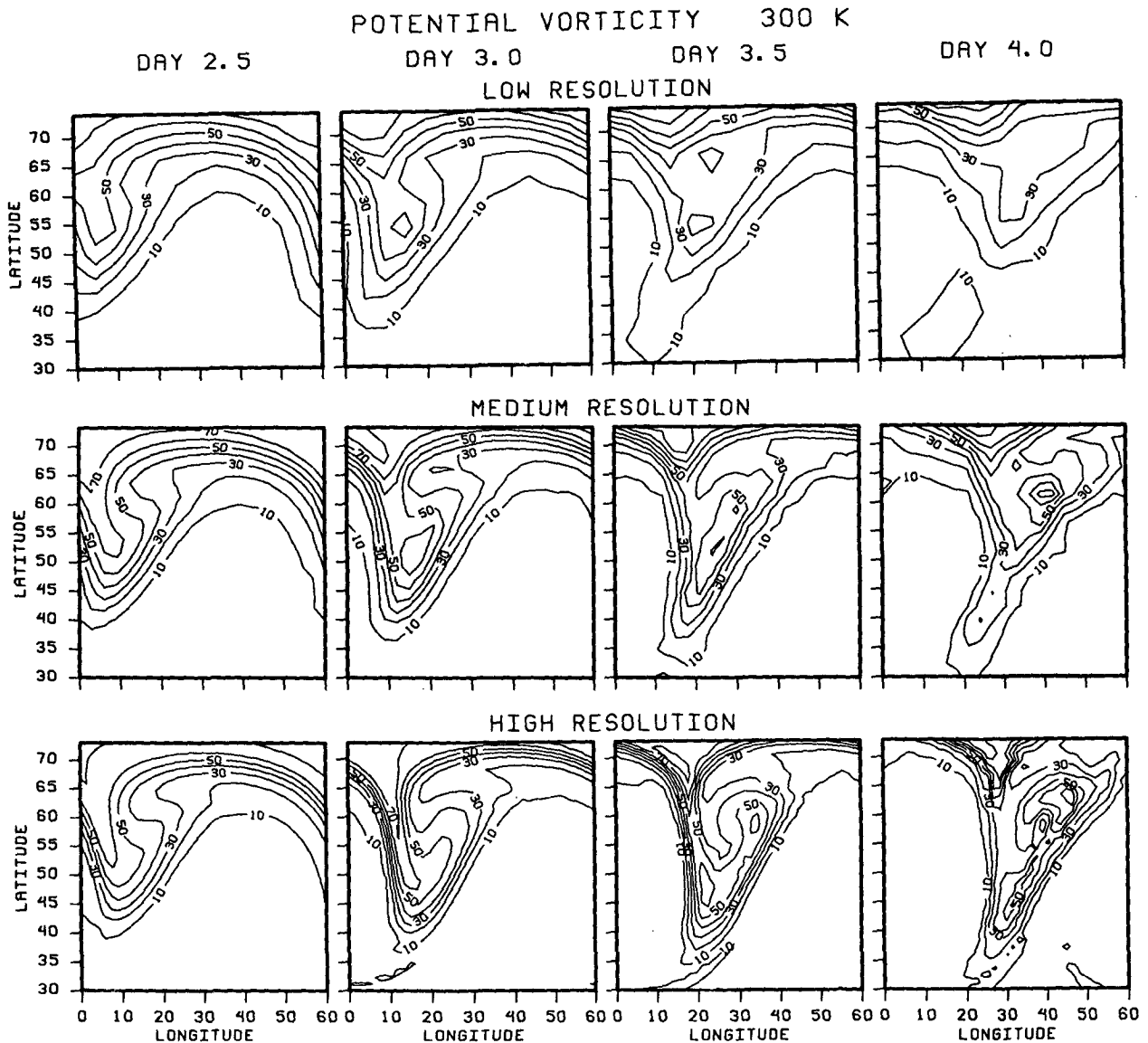


FIG. 4. Longitude-latitude contour plots of potential vorticity ( $10^{-7} \text{ K m}^2 \text{ kg}^{-1} \text{ s}^{-1}$ ) on the  $\theta = 300 \text{ K}$  surface for days 2.5, 3, 3.5, and 4 obtained with the low, medium, and high horizontal resolution versions of the model. The contour interval is  $10 \times 10^{-7} \text{ K m}^2 \text{ kg}^{-1} \text{ s}^{-1}$ .

to conditions on the distributions of both the initial zonally symmetric flow and perturbation. Our goal is to obtain unstable waves with small meridional phase tilt in the midtroposphere, at least in the initial stages of the simulations.

We start by considering the phase speed of perturbations that are locally independent of latitude on a basic state at rest. From the barotropic vorticity equation (see the Appendix), the phase speed  $\nu$  of these perturbations is

$$\nu = -\frac{2\Omega a \cos^2 \phi}{s^2}, \tag{8}$$

where  $\Omega$  and  $a$  are the angular velocity and radius of the earth, respectively, and  $s$  is the zonal wavenumber. According to (8), the magnitude of this phase speed increases toward the equator. This suggests that another velocity profile can be superimposed on profile (7) to cancel, at each latitude, the phase speed given by (8). Consequently, consider

$$\bar{u}(\phi, p) = \hat{u}(p) \sin(\pi \sin^2 \phi) + 2\Omega a \cos^3 \phi / s^2, \tag{9}$$

where  $s$  is now the wavenumber of the longest wave represented in our sector PE model. The resulting velocity distribution is shown in Fig. 6; maximum speed is  $46.2 \text{ m s}^{-1}$  at  $40^\circ$  and 200 mb.

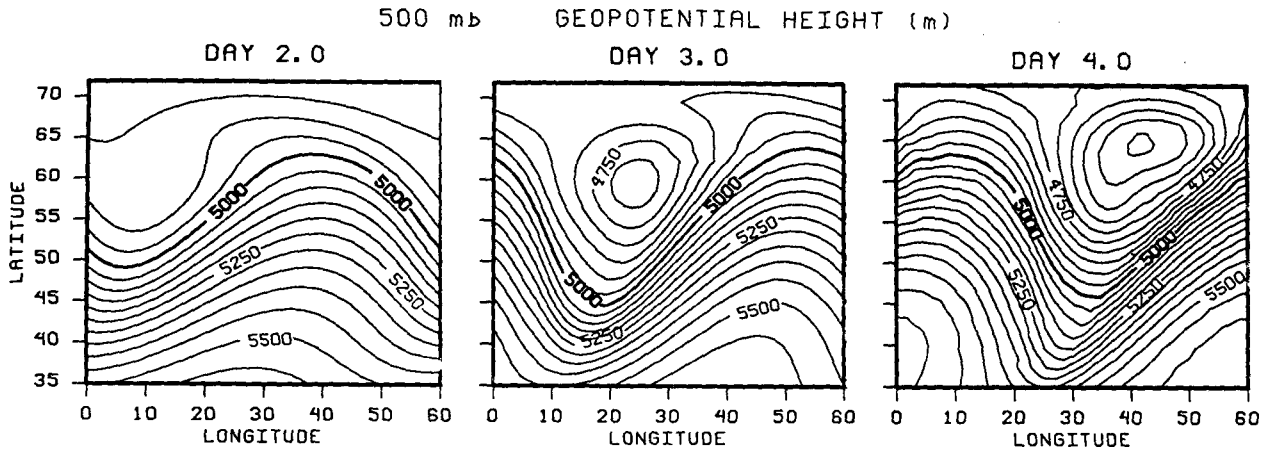


FIG. 5. Longitude-latitude contour plots of geopotential height (m) at 500 mb for days, 2, 3, and 4 obtained with the high horizontal resolution version of the model. The contour interval is 50 m. The thick contour is 5000 m.

Concerning the initial perturbation, this is taken as constant in height, with a structure corresponding to a suitable eigenfunction of the barotropic vorticity equation linearized about the mean flow (9) for  $p = 600$  mb. (Details are presented in the Appendix.) Note that this procedure can also be applied to profile (7). However, the resulting perturbation structure for profile (9)

is much simpler than that for profile (7). The wave grows slower with the former profile than with the latter profile. We will refer to the simulation with profile (9) in the initial conditions as the "control."

The potential temperature field at 400, 500, and 700 mb for day 5 of the control is shown in Fig. 7. Similar to the observed phenomenon (e.g., Shapiro 1970), the strongest gradients in potential temperature form upstream of the trough, and extend roughly parallel to the flow from just east of the thermal ridge to just east of the base of the thermal trough. The temperature gradient at 700 mb is weaker in this region than at 400 and 500 mb, so the feature does not appear connected to a lower-tropospheric front, but is rather a distinct upper-level front.

The corresponding large-scale geopotential wave has small meridional phase tilt (Fig. 8). The expected protrusion of high values of potential vorticity from the stratosphere into the upper-level frontal zone is shown in Fig. 9. The protrusion develops from subsidence in an elongated region roughly parallel to the flow upstream of the trough (Fig. 10). Similar subsidence patterns are observed by Shapiro (1970) and simulated by Mudrick (1974).

We can separate, at each point, the vertical velocity  $\omega$  into contributions by divergence of the ageostrophic wind along and across the geostrophic velocity,  $\omega_L$  and  $\omega_c$ , respectively. This separation is pertinent for our purposes since frontogenetical tilting is mainly associated with divergence of across-front flow in two-dimensional models and of along-jet flow in the conceptual model presented by Newton and Trevisan (1984a). The direction of the geostrophic wind is a good approximation to those along the jet and the front. Terms  $\omega_L$  and  $\omega_c$  are computed by vertical integration of the divergence of the corresponding wind components. The integration is carried out downward from the model top. The dominant contribution to the divergence is

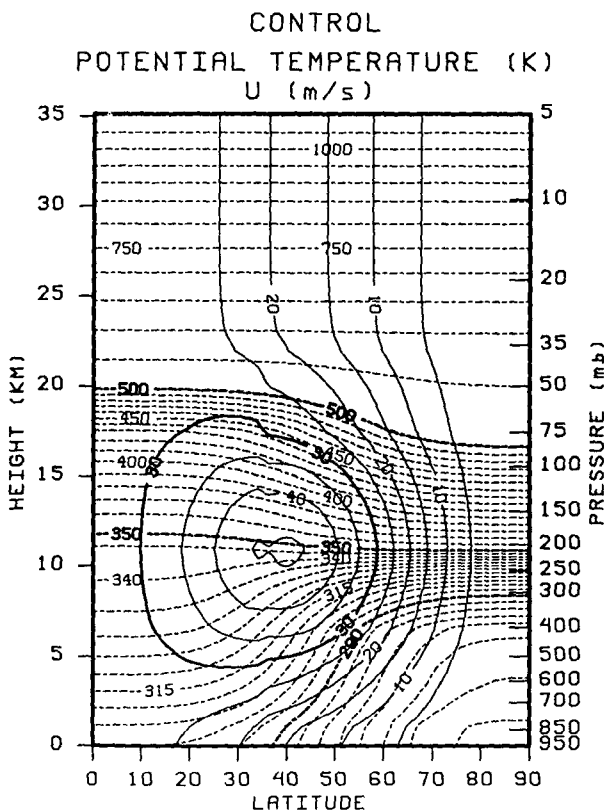


FIG. 6. As in Fig. 2, except for the control simulation.

CONTROL DAY 5.0  
POTENTIAL TEMPERATURE (K)

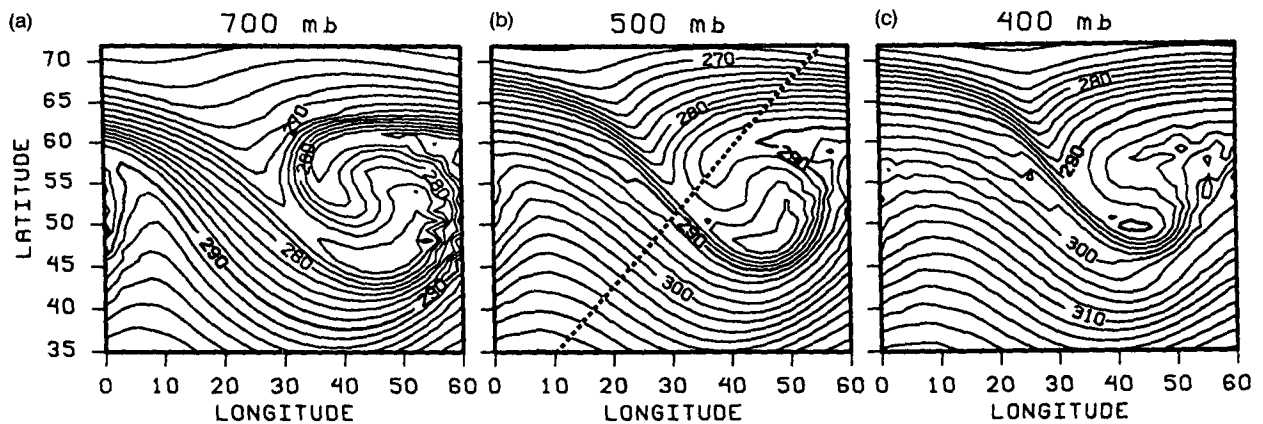


FIG. 7. Longitude-latitude contour plot of potential temperature (K) for day 5 in the Control at (a) 700 mb, (b) 500 mb, and (c) 400 mb. The contour interval is 2 K. The thick contour is 290 K. The cross section depicted in Fig. 9 is located along the dashed line.

from the upper troposphere, where changes with height of the direction of the geostrophic wind are small.

The distributions of  $\omega$ ,  $\omega_L$ , and  $\omega_c$  at 400 mb are presented in Fig. 10. There is indirect circulation along the frontal zone at this level. Comparison of the panels in this figure shows that the location of extrema for  $\omega$  are roughly those of extrema for either  $\omega_L$  or  $\omega_c$ . Near the frontal entrance region, just downstream of the ridge,  $\omega$  is mostly described in terms of  $\omega_c$ . Here the

circulation is direct equatorward of the location of maximum  $\omega$ . Just upstream of the base of the trough, the primary contribution to  $\omega$  is from  $\omega_L$  in a region

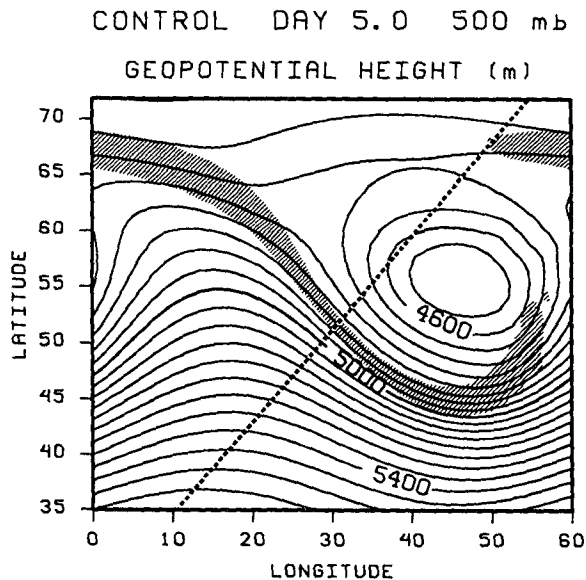


FIG. 8. Longitude-latitude contour plot of geopotential height (m) for day 5 at 500 mb. The contour interval is 50 m. The thick contour is 5000 m. Shaded regions have  $|\nabla\theta|$  greater than  $2.5 \times 10^{-5} \text{ K m}^{-1}$ . Dashed line indicates cross section.

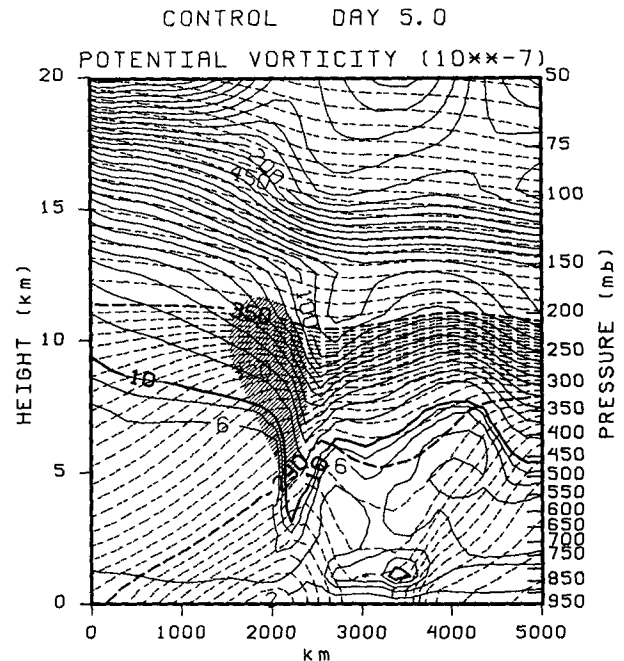


FIG. 9. Cross section of jet stream showing potential vorticity (solid lines,  $10^{-7} \text{ K m}^2 \text{ kg}^{-1} \text{ s}^{-1}$ ) and potential temperature (dashed lines, K) for day 5 in the control. Contour intervals for potential vorticity are  $2 \times 10^{-7} \text{ K m}^2 \text{ kg}^{-1} \text{ s}^{-1}$  and  $10 \times 10^{-7} \text{ K m}^2 \text{ kg}^{-1} \text{ s}^{-1}$  below and above the thick contour,  $10 \times 10^{-7} \text{ K m}^2 \text{ kg}^{-1} \text{ s}^{-1}$ . Contour intervals for potential temperature are 3 K below 350 K and 10 K above 350 K. Thick dashed lines are 290 K and 350 K. Shaded regions have wind speed greater than  $50 \text{ m s}^{-1}$ .

CONTROL DAY 4.5 400 mb

OMEGA (mb/day)

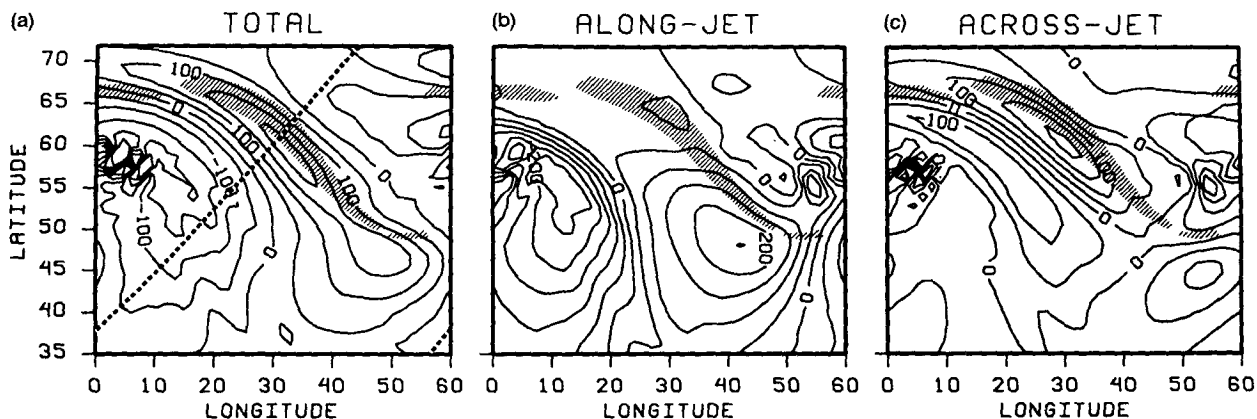


FIG. 10. Longitude-latitude contour plots at 400 mb for day 4.5 in the control of (a)  $\omega$ , (b)  $\omega_L$ , and (c)  $\omega_C$  (for definitions see the text). Units are millibars per day. The contour interval is  $50 \text{ mb day}^{-1}$ . Shaded regions have  $|\nabla\theta|$  greater than  $2.0 \times 10^{-5} \text{ K m}^{-1}$ . The cross section depicted in Fig. 12 is located along the dashed line.

of increasing cyclonic curvature and decreasing along-jet ageostrophic wind downstream. The  $\omega_C$  component is substantial near the base of the trough.

We now examine the frontogenesis processes as defined in (1). Figure 11 presents the frontogenetical contributions from tilting computed separately for  $\omega$ ,  $\omega_L$ , and  $\omega_C$ , and that from the combined effect of horizontal divergence and deformation at 400 mb. Some compensation is apparent between the horizontal and vertical advection processes. The combined effect of divergence and deformation is slightly frontogenetical near the wave ridge (situated above the surface warm front). Tilting is frontogenetical at 400 mb along most of the frontal zone in the northwesterly flow downstream of the ridge. There is substantial along-front variation of the frontogenetical contributions by  $\omega_L$  and  $\omega_C$ . The maximum frontogenesis in the upstream portion of the frontal zone is associated primarily with  $\omega_C$ . Smaller contributions to frontogenesis are provided by  $\omega_C$  near the trough and  $\omega_L$  in the downstream portion of the frontal zone. The initial development of the upstream portion of the frontal zone in this case, therefore, is primarily due to tilting associated with divergence of the across-jet ageostrophic wind. It appears that the initial frontogenesis is basically a local two-dimensional process. The contemporary study by Keyser et al. (1989) also finds the predominance of across-front tilting in upper-level frontogenesis.

The vertical velocity in a cross section perpendicular to the front about midway between the ridge and the trough is shown in Fig. 12. The presence of maximum subsidence below the jet core is consistent with the flow configuration required for Mudrick's (1974) positive-feedback process to act.

In order to test for the existence of such a positive-

feedback process in this simulation, we examine the equation for the horizontal motion in the model,

$$\frac{\partial \mathbf{v}}{\partial t} = \underbrace{-\nabla \frac{\mathbf{v}^2}{2}}_{\text{I}} - \underbrace{\zeta \mathbf{k} \times \mathbf{v}}_{\text{II}} - \underbrace{\dot{\sigma} \frac{\partial \mathbf{v}}{\partial \sigma}}_{\text{III}} - \underbrace{f \mathbf{k} \times \mathbf{v}}_{\text{IV}} - \underbrace{(\nabla g z + \alpha \nabla p)}_{\text{V}}, \quad (10)$$

where  $\sigma$  is the vertical coordinate,  $\dot{\sigma}$  is  $d\sigma/dt$ ,  $\alpha$  is the specific volume,  $z$  is geopotential height, and  $g$  is gravity. The pair of terms, I, II and term III in (10) represent the horizontal and vertical advection of momentum, respectively. Term IV represents the Coriolis acceleration and term V is the pressure gradient force. From the curl of (10), we obtain,

$$\frac{\partial}{\partial t} \zeta = \underbrace{-\nabla \zeta \cdot \mathbf{v}}_{\text{A}} - \underbrace{\zeta \nabla \cdot \mathbf{v}}_{\text{B}} - \underbrace{\nabla f \cdot \mathbf{v}}_{\text{C}} - \underbrace{f \nabla \cdot \mathbf{v}}_{\text{D}} - \underbrace{\dot{\sigma} \frac{\partial \zeta}{\partial \sigma}}_{\text{E}} + \underbrace{\mathbf{k} \cdot \left( \frac{\partial \mathbf{v}}{\partial \sigma} \times \nabla \dot{\sigma} \right)}_{\text{F}} - \underbrace{\mathbf{k} \cdot \nabla p \times \nabla \alpha}_{\text{G}}, \quad (11)$$

where terms A and B derive from II; E and F derive from III; C and D derive from IV; and G derives from V. The necessary components in the feedback are represented in (11): 1) advection of relative vorticity by the ageostrophic wind by term A, and 2) tilting by term F. Neither component is present in the quasi-geostrophic counterpart of (11).

These considerations suggest a procedure to test for the positive feedback in the simulated frontogenesis.

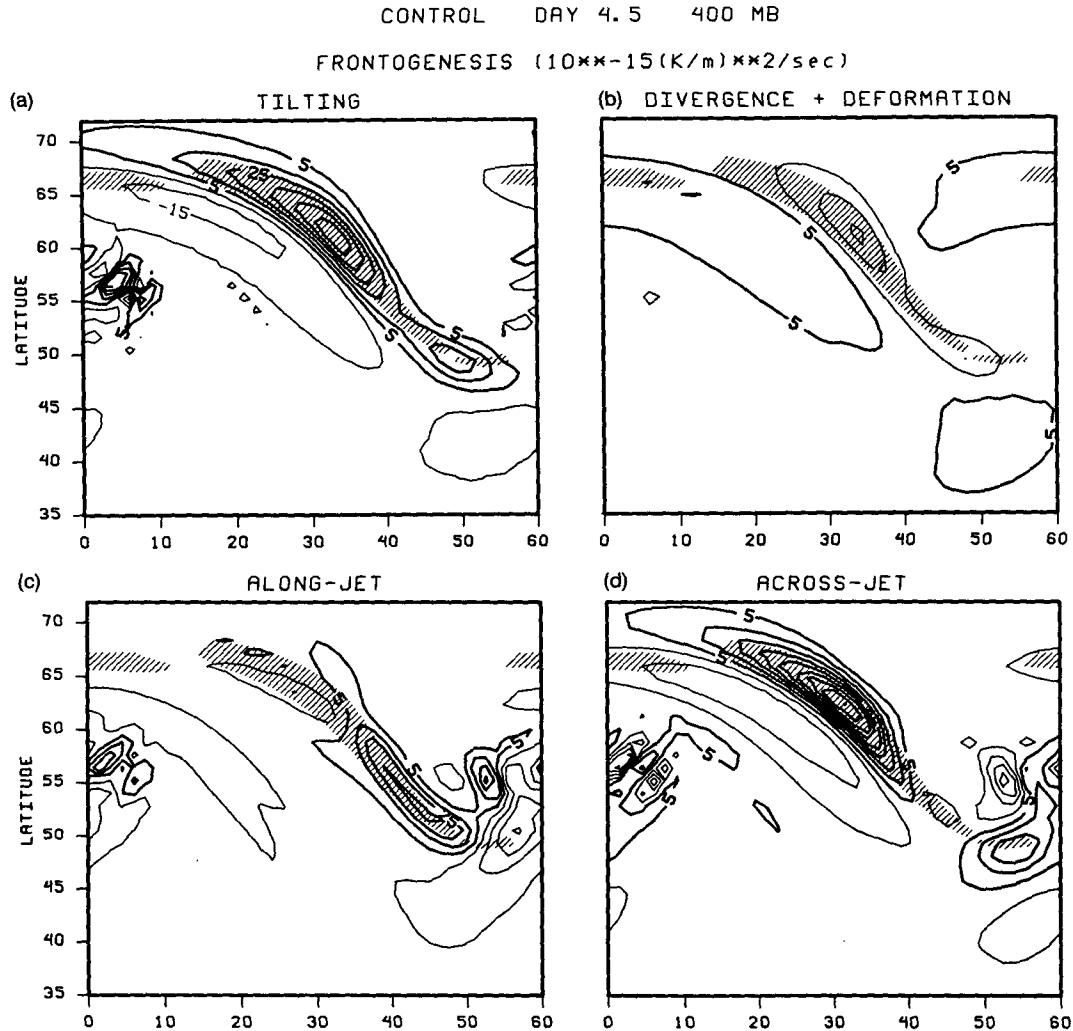


FIG. 11. Longitude-latitude contour plots of the contribution to frontogenesis ( $10^{-5} \text{K}^2 \text{m}^{-2} \text{s}^{-1}$ ) at 400 mb for day 4.5 in the control due to (a) tilting associated with  $\omega$ , (b) divergence and deformation, (c) tilting associated with  $\omega_L$ , and (d) tilting associated with  $\omega_C$ . The contour interval is  $10 \times 10^{-15} \text{K}^2 \text{m}^{-2} \text{s}^{-1}$ . Thick contours represent positive values. Shaded regions have  $|\nabla\theta|$  greater than  $2.0 \times 10^{-5} \text{K m}^{-1}$ .

The procedure consists of comparing results from the control with those obtained in simulations performed after eliminating or modifying in the model equations those terms that result in A or F in the vorticity equation. Accordingly, two sensitivity experiments are performed; experiment 1, in which the effect of tilting on the vorticity field is removed by deleting term III from the model's equations, and experiment 2, in which advection of relative vorticity by the ageostrophic wind is removed by modifying term II. If the feedback is enhancing frontogenesis, the front should be much stronger in the control than in both experiments 1 and 2.

In experiment 1, therefore, term III is set to zero in the model equation (10). No other modifications are performed. Large-scale dynamics are largely unaltered

since vertical advection of momentum can be neglected on this scale.

In experiment 2,  $v$  is replaced by the geostrophic velocity,  $v_g$ , in term II of (10), at all latitudes except in the band  $0^\circ$ – $15^\circ$ . At the grid points nearest the pole, only the meridional wind component is replaced by its geostrophic counterpart. In those locations, the zonal component of the geostrophic velocity is not defined since pressure and temperature are not specified at the pole in the finite-difference scheme. Again, large-scale dynamics are not substantially influenced by these modifications.

Experiments 1 and 2 start from the conditions in the control at day 3.5 and cover the period in which the front intensifies. This period (about 2 days long) is not long enough to exacerbate the impact on the

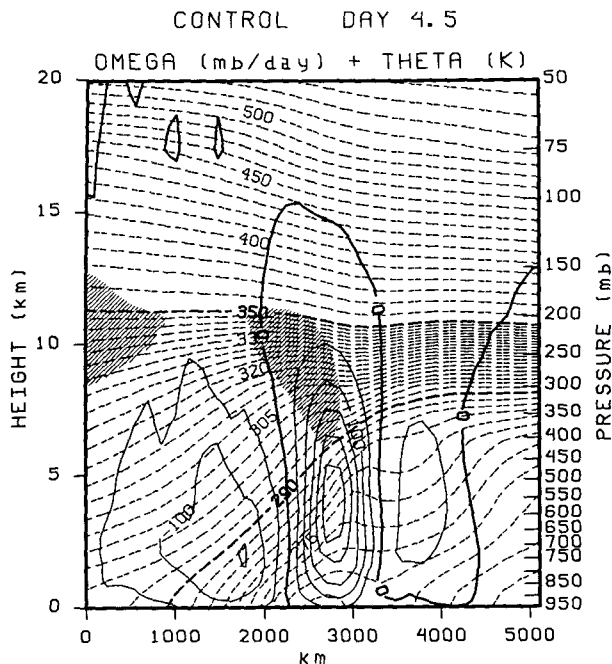


FIG. 12. Cross section of jet stream showing vertical velocity (solid lines,  $\text{mb day}^{-1}$ ) and potential temperature (dashed lines, K) for day 4.5 in the control. Contour interval for vertical velocity is  $50 \text{ mb day}^{-1}$ . The thick solid line is  $0 \text{ mb day}^{-1}$ . Intervals for potential temperature are  $3 \text{ K}$  and  $10 \text{ K}$  below and above  $350 \text{ K}$ . Thick dashed lines are  $290 \text{ K}$  and  $350 \text{ K}$ . Shaded regions have wind speed greater than  $45 \text{ m s}^{-1}$ .

synoptic-scale flow of inconsistencies induced by the artificial modifications performed on the model equations.

The magnitude of the horizontal potential temperature gradient at  $500 \text{ mb}$  for day 5 in the control and

experiments 1 and 2 is shown in Fig. 13. Note that in the control the maximum gradient is located far upstream of the trough. There is qualitative similarity between the results from the three simulations. In experiment 1, removing vertical advection of momentum reduces the  $500\text{-mb}$  maximum gradient by about 20% of that in the control (from  $4.4$  to  $3.5 \times 10^{-5} \text{ K m}^{-1}$ ). In experiment 2, removing the advection of relative vorticity by the ageostrophic wind reduces the  $500\text{-mb}$  maximum gradient in the upstream section of the front by about 17% (to  $3.7 \times 10^{-5} \text{ K m}^{-1}$ ), with lesser reductions at other levels (only about 4% at  $400 \text{ mb}$ ). Downstream of the trough, the gradient is stronger in experiment 2 than in the control.

The wind speed at  $300 \text{ mb}$  for day 5 in the control and experiments 1 and 2 is shown in Fig. 14. Again, there is a qualitative similarity between the results of all three simulations. The wind speed increases downstream in the area of frontal formation. The maximum wind speed in the control is slightly stronger than that in experiment 1 and nearly identical to that in experiment 2. The cyclonic vorticity on the poleward side of the jet is largest in the control. These results imply that vertical advection of momentum and vorticity advection by the ageostrophic wind are not crucial for the intensification of jet/front system, with the former being more important than the latter.

The quality of differences between the control simulation and experiments 1 and 2, therefore, does not provide definitive evidence that the positive-feedback process proposed by Mudrick (1974) is at work during frontal intensification. They suggest, however, that the vertical advection of momentum and vorticity advection by the ageostrophic wind are weak, albeit non-negligible, contributors to the intensification of upper-

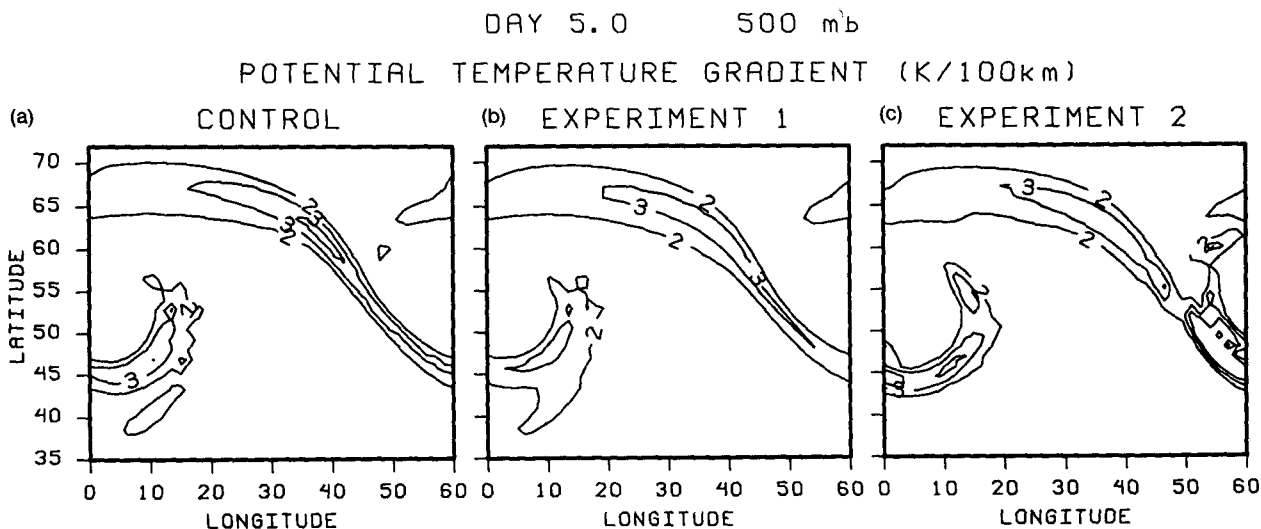


FIG. 13. Longitude-latitude contour plots of  $|\nabla\theta|$  ( $10^{-5} \text{ K m}^{-1}$ ) at  $500 \text{ mb}$  for day 5: (a) control, (b) experiment 1, (c) experiment 2. Contours are  $2.0 \times 10^{-5} \text{ K m}^{-1}$ ,  $3.0 \times 10^{-5} \text{ K m}^{-1}$ , and  $4.0 \times 10^{-5} \text{ K m}^{-1}$ .

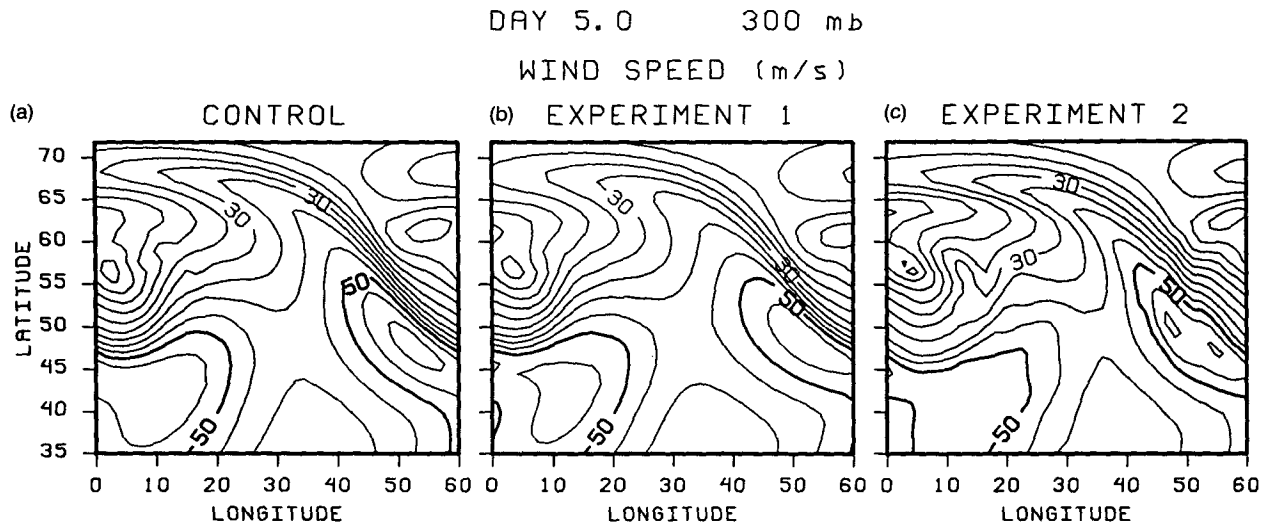


FIG. 14. As in Fig. 13, except for wind speed ( $\text{m s}^{-1}$ ) at 300 mb. The contour interval is  $5 \text{ m s}^{-1}$ . The thick contour is  $50 \text{ m s}^{-1}$ .

level frontal zones. The lack of evidence for the feedback may be related to the weak effect of tilting on the vorticity field. In the midtropospheric frontal zone, tilting is dominant in the frontogenesis equation (1), however, the tilting term in the vorticity equation (3) is an order of magnitude smaller than horizontal vorticity advection.

## 6. Summary and conclusions

Upper-level frontogenesis is generally observed to develop in the flow upstream of synoptic-scale troughs. Diagnostic studies with observational data show that an important frontogenetical process is tilting associated with indirect circulation on the poleward side of maximum subsidence. Upper-level fronts can propagate from the region of formation to downstream of the trough.

Newton and Trevisan (1984a) give a three-dimensional description of how an upper-level front/jet stream may form on a baroclinic wave. In their scenario, along-jet and across-jet ageostrophic components of the flow are both important, but on different aspects of the process. The along-jet component is important on the synoptic scale for clinogenesis (that is, increase in horizontal temperature gradient, relative vorticity, and vertical shear) upstream of the trough. The across-jet component is important on the frontal scale to increase static stability in the jet-streak entrance region. Here, frontogenetical effects of confluence and frontolytic effects of direct circulation transverse to the jet streak tend to balance for each other in the midtroposphere.

Simulations of upper-level frontogenesis with both two- and three-dimensional models are reported in the literature. In two-dimensional models, the frontoge-

netical forcing is prescribed. The simulated upper-level fronts have features that resemble those of observed fronts, particularly when the prescribed forcings include confluence across the front and cold advection along the front (Keyser and Pecnick 1985). In three-dimensional models, the development of upper-level fronts associated with synoptic-scale waves can be simulated without prescribed forcings. Previous three-dimensional studies are with  $\beta$ -plane models.

Our simulations are performed with an adiabatic, PE model on a  $60^\circ$  sector of one hemisphere. The model has 21 layers in the vertical (14 layers below 100 mb), and the horizontal resolution is  $1.2^\circ \text{ lat} \times 1.5^\circ \text{ long}$ . We showed that versions of the model with lower horizontal resolution yield less adequate representations of the developing frontal zones.

The results of simulations from initial conditions corresponding to wind profiles symmetric about the latitude of maximum wind at each pressure level show that growing baroclinic waves develop significant southwest-northeast phase tilt. The strongest frontal zones in the midtroposphere develop downstream of the trough in these cases. We could simulate strong frontal zones developing upstream of wave troughs by specially designing the initial conditions, comprising both the initial zonal flow and the perturbation, to produce small phase tilt. These results suggest that the answer to the first issue raised in the Introduction is that *there can be significant differences between simulations of frontogenesis from different initial conditions*.

Our results suggest that the role played in upper-level frontogenesis by divergence of the along-jet ageostrophic wind is not as important as in the conceptual model proposed by Newton and Trevisan (1984a). We obtain that the primary contributor to

the frontogenetical tilting effect in the upstream portion of the frontal zone is the vertical velocity associated with divergence of the *across-jet* ageostrophic wind. Tilting associated with divergence of the *along-jet* ageostrophic wind also enhances frontogenesis, but to a lesser degree, farther downstream along the frontal zone. Thus, our results suggest that the answer to the second issue raised in the Introduction is that *upper-level frontogenesis can be largely a two-dimensional process, at least locally*. We should emphasize, however, that development of this two-dimensional process highly depends on the three-dimensional structure of the developing baroclinic wave.

Concerning the third issue raised in the Introduction, *our results do not provide definitive evidence that the vertical advection of momentum and horizontal advection of vorticity by the ageostrophic wind are components in a positive feedback at work for the intensification of upper-level frontal zones. Nevertheless, the results suggest that those processes are nonnegligible contributors to the intensification*. These conclusions are based on the comparisons between a control simulation and experiments in which the model equations were modified to eliminate necessary components for the feedback. The former component is found to be somewhat more important than the latter component.

To gain insight into the weak effect of vorticity advection by the ageostrophic wind, we examine the relative contributions to vorticity advection by the geostrophic and ageostrophic velocity components. We refer to these contributions as follows:

$$-\nabla\zeta \cdot \mathbf{v} = -\nabla\zeta \cdot \mathbf{v}_g - \nabla\zeta \cdot \mathbf{v}_a, \quad (12)$$

where  $\mathbf{v}_a$  is the ageostrophic velocity. The first and second terms on the right-hand side of (12) are of order  $VZ/L$  and  $V_a Z/N$ , respectively, where  $V$  and  $V_a$  are the scales of along-jet geostrophic wind and across-jet ageostrophic wind, respectively;  $Z$  is the scale of relative vorticity;  $L$  is the length scale of along-jet motions (the synoptic-scale length); and  $N$  is the across-jet scale of the jet/frontal system. As horizontal shear is large near the jet,  $Z$  is set equal to  $V/N$ . For the ageostrophic component of vorticity advection to be as large as or larger than the geostrophic component,  $V_a$  must satisfy the following relation,

$$V_a \geq \frac{VN}{L} = \frac{V^2}{LZ}. \quad (13)$$

Reasonable values for  $L$  and  $Z$  are  $10^6$  m and  $10^{-4}$   $s^{-1}$ . In jet streams, where the wind speed can easily exceed  $50$   $m\ s^{-1}$ , a reasonable value for  $V^2$  is  $1000$   $m^2\ s^{-2}$  (Shapiro 1970). From (13) we obtain that the magnitude of the across-jet ageostrophic flow must be about  $10$   $m\ s^{-1}$ . This is not an unreasonable value since Uccellini et al. (1984), Uccellini and Kocin (1987), and Cammas and Raymond (1989) observe cases of across-jet ageostrophic winds exceeding  $10$  m

$s^{-1}$ . In our simulation, however, the maximum values are about  $5$   $m\ s^{-1}$ .

The question remains whether qualitatively different results can be obtained by substantially increasing the resolution of the model. Concerning the vertical resolution, the control case run with both the 14- and 21-layer versions produced upper-level fronts of about the same intensity. However, the vorticity advection by the ageostrophic wind increased in relative importance with increased vertical resolution. The analysis of these questions provides the motivation for our current research.

*Acknowledgments.* It is a pleasure to thank A. Arakawa and D. Keyser for stimulating discussion on the upper-level frontogenesis problem. We also thank C. Konor for his comments on the manuscript. The research was supported by NSF under Grant ATM 88-22729. The simulations were performed at the computer facility of NCAR.

## APPENDIX

### Initial Perturbations

The initial perturbations to the zonal flow can be formulated so as to reduce the barotropic tendency for waves to tilt in the meridional direction. As a basis for determining the structure of these perturbations, we examine the linearized barotropic vorticity equation,

$$\frac{\partial}{\partial t} \nabla^2 \psi' = -\frac{\bar{u}}{a \cos(\phi)} \frac{\partial \zeta'}{\partial \lambda} - \frac{v'}{a} \left[ \frac{\partial \bar{\zeta}}{\partial \phi} + 2\Omega \cos(\phi) \right], \quad (A1)$$

where  $\bar{u}$  is the basic state wind,  $\bar{\zeta}$  is the zonal-mean relative vorticity of the basic state,  $v'$  is the northward component of the perturbation velocity,  $\psi'$  is the streamfunction of the perturbation flow,  $\zeta'$  is the perturbation vorticity, and  $\lambda$  is longitude. We take 600 mb as the reference level. Substitution of

$$\psi'(\lambda, \phi, t) = \Psi(\phi) e^{i(s\lambda - \nu t)}, \quad (A2)$$

where  $\nu$  is the phase speed, into (A1) yields

$$\frac{d}{d\phi} \left[ \cos(\phi) \frac{d\Psi}{d\phi} \right] + A(\phi)\Psi = 0, \quad (A3)$$

where

$$A(\phi) = -\frac{s^2}{\cos(\phi)} + \left\{ -2\Omega s \cos(\phi) + \frac{s}{a} \frac{\partial}{\partial \phi} \left[ \frac{1}{\cos(\phi)} \frac{\partial}{\partial \phi} [\bar{u} \cos(\phi)] \right] \right\} \times \left[ \nu - \frac{\bar{u}s}{a \cos(\phi)} \right]^{-1}. \quad (A4)$$

The eigenvalue  $\nu$  is computed by approximating the latitudinal derivatives with finite differences in a grid

consistent with that used in the GCM and solving for the determinant equal to zero. By this method, several eigenfunctions are available for a given initial flow. After an appropriate eigenfunction is selected, the perturbation amplitude of the geopotential height  $z'$  is obtained as

$$gz' = f\psi'. \quad (\text{A5})$$

The structure found in pressure surfaces is then interpolated to the  $\sigma$  surfaces of the model.

#### REFERENCES

- Arakawa, A., and V. R. Lamb, 1977: Computational design of the basic dynamical process of the University of California, Los Angeles general circulation model. *Methods in Computational Physics*, Academic Press, 173–275.
- , and —, 1981: A potential enstrophy and energy conserving scheme for the shallow-water equations. *Mon. Wea. Rev.*, **109**, 18–36.
- , and M. J. Suarez, 1983: Vertical differencing of the primitive equations in sigma coordinates. *Mon. Wea. Rev.*, **111**, 34–45.
- Bosart, L. F., 1970: Mid-tropospheric frontogenesis. *Quart. J. Roy. Meteor. Soc.*, **96**, 422–471.
- Buzzi, A., T. Nanni and M. Tagliuzuca, 1977: Mid-tropospheric frontal zones: Numerical experiments with an isentropic coordinate primitive equation model. *Arch. Meteor. Geophys. Bioklim.*, **A26**, 155–178.
- , A. Trevisan and G. Salustri, 1981: Internal frontogenesis: A two-dimensional model in isentropic, semigeostrophic coordinates. *Mon. Wea. Rev.*, **109**, 1053–1060.
- Cammas, J., and D. Raymond, 1989: Analysis and diagnosis of the composition of ageostrophic circulations in jet-front systems. *Mon. Wea. Rev.*, **117**, 2447–2462.
- Danielsen, E. F., 1968: Stratospheric-tropospheric exchange based on radioactivity, ozone, and potential vorticity. *J. Atmos. Sci.*, **25**, 502–518.
- Eliassen, A., 1962: On the vertical circulation in frontal zones. *Geofys. Publ.*, **24**, 147–160.
- Hollingsworth, A., 1975: Baroclinic instability of a simple flow on the sphere. *Quart. J. Roy. Meteor. Soc.*, **101**, 495–528.
- , A. J. Simmons and B. J. Hoskins, 1976: The effect of spherical geometry on momentum transports in simple baroclinic flows. *Quart. J. Roy. Meteor. Soc.*, **102**, 901–911.
- Hoskins, B. J., 1971: Atmospheric frontogenesis models: Some solutions. *Quart. J. Roy. Meteor. Soc.*, **97**, 139–153.
- , 1972: Non-Boussinesq effects and further development in a model of upper tropospheric frontogenesis. *Quart. J. Roy. Meteor. Soc.*, **98**, 532–541.
- , 1975: The geostrophic momentum approximation and the semi-geostrophic equations. *J. Atmos. Sci.*, **32**, 233–242.
- , and F. P. Bretherton, 1972: Atmospheric frontogenesis models: Mathematical formulation and solution. *J. Atmos. Sci.*, **29**, 11–37.
- Keyser, D., and M. J. Pecnick, 1985: A two-dimensional primitive-equation model of frontogenesis forced by confluence and horizontal shear. *J. Atmos. Sci.*, **42**, 1259–1282.
- , and M. A. Shapiro, 1986: A review of the structure and dynamics of upper-level frontal zones. *Mon. Wea. Rev.*, **114**, 452–499.
- , B. D. Schmidt and D. G. Duffy, 1989: A technique for representing three-dimensional vertical circulations in baroclinic disturbances. *Mon. Wea. Rev.*, **117**, 2463–2494.
- Krisnamurti, T. N., 1968: A study of a developing wave cyclone. *Mon. Wea. Rev.*, **96**, 208–217.
- Manabe, S., J. L. Holloway, Jr. and H. M. Stone, 1970: Simulated climatology of a general circulation model with a hydrologic cycle cycle. III: Effects of increased horizontal computational resolution. *Mon. Wea. Rev.*, **98**, 175–212.
- Mechoso, C. R., K. Yamazaki, A. Kitoh and A. Arakawa, 1985: Numerical forecasts of stratospheric warming events during the winter of 1979. *Mon. Wea. Rev.*, **113**, 1015–1029.
- Mudrick, S. E., 1974: A numerical study of frontogenesis. *J. Atmos. Sci.*, **31**, 869–892.
- Namias, J., and F. P. Clapp, 1949: Confluence theory of the high tropospheric jet stream. *J. Meteor.*, **6**, 330–336.
- Newton, C. W., 1954: Frontogenesis and frontolysis as a three-dimensional process. *J. Meteor.*, **11**, 449–461.
- , and A. Trevisan, 1984a: Clinogenesis and frontogenesis in jet-stream waves. Part I: Analytical relations to wave structure. *J. Atmos. Sci.*, **41**, 2717–2734.
- , and —, 1984b: Clinogenesis and frontogenesis in jet-stream waves. Part II: Channel model numerical experiments. *J. Atmos. Sci.*, **41**, 2735–2755.
- Oort, A. H., 1983: Global atmospheric circulation statistics, 1958–1973. NOAA Prof. Pap. 14, 180 pp. [NTIS PB84-129717]
- Palmén, E., 1951: The role of atmospheric disturbances in the general circulation. *Quart. J. Roy. Meteor. Soc.*, **77**, 337–354.
- , and C. W. Newton, 1969: Atmospheric circulation systems. Academic Press, 603 pp.
- Reed, R. J., 1955: A study of a characteristic type of upper-level frontogenesis. *J. Meteor.*, **12**, 226–237.
- , and F. Sanders, 1953: An investigation of the development of a mid-tropospheric frontal zone and its associated vorticity field. *J. Meteor.*, **10**, 338–349.
- , and E. F. Danielsen, 1959: Fronts in the vicinity of the tropopause. *Arch. Meteor. Geophys. Bioklim.*, **A11**, 1–17.
- Reeder, M. J., and D. Keyser, 1988: Balanced and unbalanced upper-level frontogenesis. *J. Atmos. Sci.*, **45**, 3366–3386.
- Shapiro, M. A., 1970: On the applicability of the geostrophic approximation to upper-level frontal-scale motion. *J. Atmos. Sci.*, **27**, 408–420.
- , 1975: Simulation of upper-level frontogenesis with a 20-level isentropic coordinate primitive equation model. *Mon. Wea. Rev.*, **103**, 591–604.
- , 1978: Further evidence of the mesoscale and turbulent structure of upper-level jet stream-frontal zone systems. *Mon. Wea. Rev.*, **106**, 1100–1111.
- , 1981: Frontogenesis and geostrophically forced secondary circulations in the vicinity of jet stream-frontal zone systems. *J. Atmos. Sci.*, **38**, 954–973.
- Simmons, A. J., and B. J. Hoskins, 1977: Baroclinic instability on the sphere: Solutions with a more realistic tropopause. *J. Atmos. Sci.*, **34**, 581–588.
- , and —, 1978: The life cycles of some nonlinear baroclinic waves. *J. Atmos. Sci.*, **35**, 414–432.
- Staley, D. O., 1960: Evaluation of potential-vorticity changes near the tropopause and the related vertical motions, vertical advection of vorticity, and transfer of radioactive debris from stratosphere to troposphere. *J. Meteor.*, **17**, 591–620.
- Suarez, M. J., A. Arakawa and D. A. Randall, 1983: The parameterization of the planetary boundary layer in the UCLA general circulation model: Formulation and results. *Mon. Wea. Rev.*, **111**, 2224–2243.
- Uccellini, L. W., P. J. Kocin, R. A. Petersen, C. H. Wash and K. F. Brill, 1984: The President's Day cyclone of 18–19 February 1979: Synoptic overview and analysis of the subtropical jet streak influencing the precyclogenetic period. *Mon. Wea. Rev.*, **112**, 31–55.
- , D. Keyser, K. F. Brill and C. H. Wash, 1985: The President's Day cyclone of 18–19 February 1979: Influence of upstream trough amplification and associated tropopause folding on rapid cyclogenesis. *Mon. Wea. Rev.*, **113**, 962–988.
- , and P. J. Kocin, 1987: The interaction of jet stream circulations during heavy snow events along the east coast of the United States. *Wea. Forecasting*, **2**, 289–308.